

Control of interannual and longer-term variability of stratospheric water vapor

S. Fueglistaler

Department of Atmospheric Sciences, University of Washington, Seattle, Washington, USA

P. H. Haynes

Department of Applied Mathematics and Theoretical Physics, University of Cambridge, Cambridge, UK

Received 24 March 2005; revised 5 September 2005; accepted 28 September 2005; published 23 December 2005.

[1] We use trajectory calculations based on 40-year European Reanalysis (ERA-40) data to predict the water mixing ratio of air entering the stratosphere in the tropics ($[\text{H}_2\text{O}]_e$) and thereby to examine interannual and longer-term changes. $[\text{H}_2\text{O}]_e$ is determined from the saturation mixing ratio of the coldest point during ascent from the troposphere to the stratosphere (the Lagrangian cold point). These model predictions for the time variation of $[\text{H}_2\text{O}]_e$ agree very well with a broad range of measurements (Stratospheric Aerosol and Gas Experiment (SAGE) II, Halogen Occultation Experiment (HALOE), Microwave Limb Sounder (MLS), and Atmospheric Trace Molecule Spectroscopy (ATMOS)). During periods when measurements are consistent among various sensors and ERA-40 temperatures show good agreement with radiosondes (1995–2002), the correlation between model predictions and HALOE water vapor anomalies in the tropical lower stratosphere is $r = 0.81$, as high as that between HALOE and SAGE II ($r = 0.8$). The model predictions suggest that the stratospheric quasi-biennial oscillation, El Niño–Southern Oscillation, and possibly volcanic eruptions all play a significant role in modulating $[\text{H}_2\text{O}]_e$, leading to interannual anomalies of order 0.5 ppmv with timescales of several months to years. Although the Lagrangian calculations show substantial interannual variability of transport pathways into the stratosphere, the results show that the interannual anomalies of $[\text{H}_2\text{O}]_e$ are dominated by anomalies of the zonal mean temperature rather than by transport changes or localized temperature anomalies. This reinforces the paradox of apparently increasing stratospheric water vapor concentrations alongside, if anything, slightly decreasing temperatures at the tropical tropopause. The combination of measurement uncertainties and relatively strong interannual variability with periods of several months to years, on the one hand, limits our ability to detect, attribute, and verify long-term trends and, on the other hand, raises the question as to whether the previously published estimates of long-term trends are too large.

Citation: Fueglistaler, S., and P. H. Haynes (2005), Control of interannual and longer-term variability of stratospheric water vapor, *J. Geophys. Res.*, 110, D24108, doi:10.1029/2005JD006019.

1. Introduction

[2] Stratospheric water vapor plays an important role for the radiation budget of the troposphere [Held and Soden, 2000] as well as the stratosphere [Forster and Shine, 2002] and for stratospheric chemistry, in particular for ozone [Evans *et al.*, 1998; Dvortsov and Solomon, 2001]. Water vapor enters the stratospheric “overworld” (the part of the stratosphere above 380 K potential temperature [Holton *et al.*, 1995]) through troposphere-to-stratosphere transport of air primarily in the tropics. It is widely agreed that the water vapor mixing ratio of air entering the stratosphere (henceforth $[\text{H}_2\text{O}]_e$) is limited to a few parts per million by volume

(ppmv) by the extremely low temperatures at the tropical tropopause, but the details of the processes that control $[\text{H}_2\text{O}]_e$ remain controversial [Newell and Gould-Stewart, 1981; Danielsen, 1993; Sherwood and Dessler, 2000; Holton and Gettelman, 2001]. Recently, Fueglistaler *et al.* [2005] have shown that annual mean and seasonal cycle of $[\text{H}_2\text{O}]_e$ can be explained to within ~ 0.2 ppmv by synoptic-scale temperature and winds, provided the full four-dimensional temperature history of air entering the stratosphere is taken into account.

[3] In addition to the seasonal cycle, there is significant interannual variability of stratospheric water vapor [e.g., Randel *et al.*, 2004], and there is also some evidence for a long-term positive trend [Oltmans *et al.*, 2000; Rosenlof *et al.*, 2001]. In this paper we present an analysis of interannual to multidecadal variability of stratospheric water vapor

concentrations, and of their governing processes. We use the trajectory calculations of tropical troposphere-to-stratosphere transport (TST) of *Fueglistaler et al.* [2005] for the period 1979–2002 to predict $[\text{H}_2\text{O}]_e$, and analyze the processes controlling interannual variability in the model calculations. Systematic differences between model calculations and observations may be taken as indicative of processes affecting $[\text{H}_2\text{O}]_e$ not taken into account in the model calculations.

[4] To focus ideas, let $F = F_1 + F_2$ be the total mass flux into the tropical stratosphere, and F_1 be the mass flux resolved by the model calculations, whereas F_2 is the mass flux due to unresolved processes. Then the total water flux is $F_1 \cdot \chi_1 + F_2 \cdot \chi_2$, where χ_1 is the water vapor mixing ratio predicted by the model calculations, and χ_2 is the (unknown) water vapor mixing ratio of the unresolved flux. This decomposition allows one to account for systematic differences between χ_1 and χ_2 , and the (true) entry mixing ratio may be written as

$$[\text{H}_2\text{O}]_e = f_1 \cdot \chi_1 + f_2 \cdot \chi_2 \quad (1)$$

where $f_1 \equiv F_1/F$ is the fraction of TST that is resolved, and $f_2 = 1 - f_1$ is the fraction not resolved by the model calculations. The trajectory calculations used here are based on wind and temperature fields of the reanalysis project, 40-year European Reanalysis (ERA-40) [*Simmons and Gibson, 2000*], of the European Centre for Medium-Range Weather Forecasts (ECMWF). Thus F_1 is the mass flux into the tropical stratosphere as represented in ERA-40, and F_2 is the flux due to processes not or poorly resolved in ERA-40, for example individual convective cells penetrating the tropopause. The model calculations then further assume that tropical cirrus clouds typically dehydrate the air to the saturation mixing ratio (χ^{sat}) of the synoptic-scale temperature field, and consequently the mixing ratio of tropical TST upon entry into the stratosphere is determined by the minimum saturation mixing ratio encountered during ascent, i.e.,

$$\chi_1 = \min(\chi^{\text{sat}}(T_{\text{syn}})) + \epsilon, \quad (2)$$

$$\epsilon \ll \min(\chi^{\text{sat}}(T_{\text{syn}})) \quad (3)$$

where the synoptic temperature T_{syn} is the temperature field as resolved by ERA-40. The model calculations employed here deliberately simplify many aspects of cloud microphysics and mesoscale dynamics (that affect ϵ in the equation above), and reflect essentially synoptic-scale dynamics and temperature fields in the tropical upper troposphere and lower stratosphere. For these calculations *Fueglistaler et al.* [2005] determined the total residual due to unresolved transport and simplifications $f_1 \cdot \epsilon + f_2 \cdot \chi_2 \simeq 0.2$ ppmv, or about 5% of $[\text{H}_2\text{O}]_e$. It may be that one reason that the residual is small is that there are some cancelling effects between different neglected processes, in particular between incomplete sedimentation of cirrus clouds (that might imply positive ϵ) and the effect of mesoscale temperature fluctuations (e.g., due to gravity waves) that would tend to lower the minimum temperature compared to

that of the synoptic-scale field (and hence might imply negative ϵ in the formulation above).

[5] In assuming $f_1 = 1$ and $\epsilon = 0$ the model calculations represent only interannual variability due to temperature variability and transport pathway variability of tropical TST as resolved by ERA-40. In particular the model calculations do not consider processes that could induce variability or longer-term changes in ϵ , or in the contribution to stratospheric water vapor from the unresolved flux ($f_2 \cdot \chi_2$).

[6] The paper is organized as follows. Section 2 presents the data and the method to predict $[\text{H}_2\text{O}]_e$. Section 3 compares the model predictions for $[\text{H}_2\text{O}]_e$ and water vapor mixing ratios in the lower tropical stratosphere to spaceborne observations beginning in 1986, and section 4 analyzes the processes governing interannual variability in the model calculations. Section 5 discusses the role of tropical zonal mean temperature anomalies (as opposed to localized temperature trends or transport anomalies) for $[\text{H}_2\text{O}]_e$ anomalies. Employing a simple model for transport and chemistry in the stratosphere, we further compare in section 6 the model predictions to measurements in the midlatitude stratosphere. Section 7 recapitulates the results of the extensive comparisons presented in earlier sections, and discusses their implications for multidecadal trends. Section 8 finally provides a summary and conclusions.

2. Method and Data

2.1. Water Vapor Measurements

[7] Measurements of water vapor in the tropical lower stratosphere with sufficient temporal and spatial resolution to calculate reliable tropical monthly mean values exist from spaceborne observations only. Here we use water vapor measurements from the Stratospheric Aerosol and Gas Experiment (SAGE) II (data version 6.20 [*Thomason et al., 2004*]) from 1985 to present, from Halogen Occultation Experiment (HALOE) [*Russell et al., 1993*] version 19 data from 1991 to present, and from the Microwave Limb Sounder (MLS) data version v7.02 [*Read et al., 2004*] for the period September 1991 to April 1993. In addition, we will refer to the estimates of $[\text{H}_2\text{O}]_e$ from the Atmospheric Trace Molecule Spectroscopy (ATMOS) missions as published by *Michelsen et al.* [2000] and to the NOAA frost point hygrometer measurements [*Oltmans et al., 2000*] at midlatitude sites (Washington, D. C., and Boulder, Colorado, USA).

[8] The accuracy of these instruments, and concerns about unresolved discrepancies among various instruments has been discussed elsewhere [*Kley et al., 2000*]. In general, HALOE v19 water vapor data are considered as fairly accurate when compared with in situ measurements, with HALOE being typically about 10% drier. The SAGE II water vapor has been updated since the SPARC assessment to version 6.2. This version shows good agreement both with in situ observations and HALOE, and effectively resolves the bias observed in earlier versions [*Thomason et al., 2004*]. The MLS water vapor product has been updated to version V7.02, which shows good agreement with HALOE and frost point hygrometers. In particular, the seasonal evolution of zonal means are accurate within 10%, but have a dry bias at 100 hPa of about 20% [*Read et al., 2004*], for which the data shown below have been corrected.

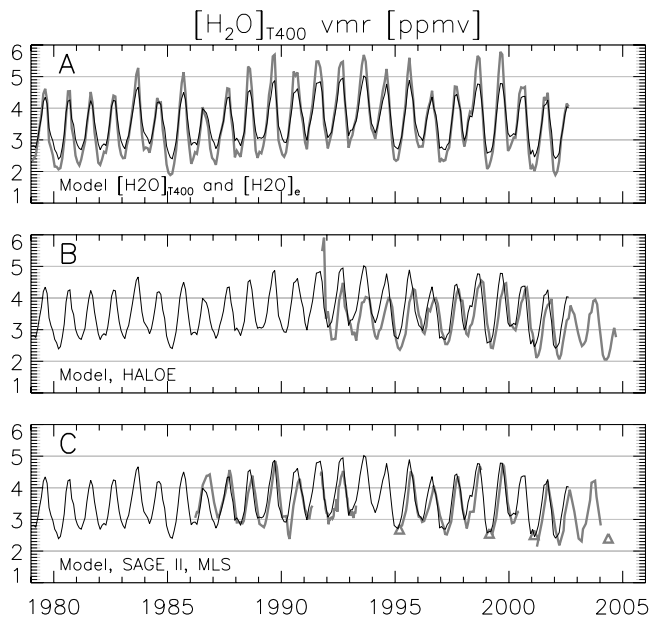


Figure 1. Tropical mean (30°S to 30°N) water vapor mixing ratios in the lowermost stratosphere at 400 K ($[\text{H}_2\text{O}]_{\text{T}400}$). (a) Model results (black) and model results for $[\text{H}_2\text{O}]_{\text{e}}$ (grey). (b) Model results (black) and HALOE observations (grey). (c) Model results (black), SAGE II (grey), and MLS (grey, 1991–1993).

However unresolved differences between measurements by in situ and remote-sensing instruments as presented in Figure 1 of the SPARC assessment of UT/LS water vapor [Kley *et al.*, 2000] remain an important point of concern and need to be resolved (E. Weinstock, personal communication, 2005). Further, the limited vertical resolution of the instruments (about 2 km for HALOE, 1 km for SAGE II, and 3–4 km for MLS) constrains the conclusions that can be drawn from a comparison with model data on a particular potential temperature surface. However, as most of the discussion presented here focusses on interannual anomalies rather than (absolute) monthly mean water vapor mixing ratios, the implications of possible biases of HALOE, MLS and SAGE II are not so severe, as long as the instruments do not show a drift over time and the signal (the anomalies) to noise (arising from measurement errors and inhomogeneous sampling) ratio is sufficiently high.

[9] The construction of a reliable tropical mean water vapor mixing ratio on the timescale of a month is a challenging task for the observations based on solar occultation (i.e., HALOE and SAGE II; MLS provides sufficiently high temporal and spatial sampling, with about 1300 profiles per day, for a straightforward averaging procedure). Following the method outlined by Randel *et al.* [1998], we calculate monthly mean values for a number of discrete (spatial) grid cells on the 400 K isentropic surface and perform a least squares fit (for each grid cell) with a harmonic signal with periods of 12, 6 and 3 months. For each grid cell, we then calculate the monthly anomaly as the difference between its actually observed mean mixing ratio and the expected value from the climatological annual cycle for the corresponding time of year and grid cell. Finally, the

climatological tropical annual cycle is the average of the climatological annual cycle of each grid cell, and the monthly mean anomaly is the average of the anomalies of each grid cell of the corresponding month.

2.2. Model Calculations

[10] We estimate $[\text{H}_2\text{O}]_{\text{e}}$ from the temperature histories of tropical TST, calculated from trajectories based on 6-hourly wind and temperature fields from the reanalysis project ERA-40, arguably one of the best currently available reconstructions of the recent atmosphere. The trajectory calculations are those used previously by Fueglistaler *et al.* [2005]. Backward trajectories are started at the end of every month on a $2^{\circ} \times 2^{\circ}$ grid between 30°S and 30°N on 400 K potential temperature (lower tropical stratosphere) and traced back in time over 3 months, for the period 1979 (beginning of satellite observations) to August 2002 (end of ERA-40 data).

[11] Within the total ensemble of trajectories, we identify TST trajectories as those that rise from below 340 K to 400 K [Fueglistaler *et al.*, 2004]. We define the point of minimum saturation mixing ratio along TST trajectories as the “Lagrangian cold point” [Fueglistaler *et al.*, 2005], that reflects the full four-dimensional temperature history of tropical TST (as represented in the trajectory calculations), in contrast to the conventional cold point that refers to the coldest temperature of a vertical temperature profile.

[12] A detailed description of the method to predict entry mixing ratio $[\text{H}_2\text{O}]_{\text{e}}$ and tropical mean mixing ratio at 400 K $[\text{H}_2\text{O}]_{\text{T}400}$ (which requires assigning climatological water vapor mixing ratios to non-TST trajectories) is given by Fueglistaler *et al.* [2005]. In addition to observations in the tropics, we will further use water vapor measurements in the midlatitude stratospheric overworld ($[\text{H}_2\text{O}]_{\text{o}}$) to assess and constrain the model calculations of $[\text{H}_2\text{O}]_{\text{e}}$. We use a simple model to predict $[\text{H}_2\text{O}]_{\text{o}}(t)$ that convolves the model estimates of $[\text{H}_2\text{O}]_{\text{e}}(t)$ with a stratospheric age spectrum and adds the water vapor contribution resulting from methane oxidation during stratospheric transport. Further details are given in section 6.

2.3. Accuracy of ERA-40 Temperatures

[13] The assessment of the model calculations, and the resulting conclusions, critically depend on the accuracy of the underlying temperature field of the ERA-40 data around the tropical tropopause. A short discussion of the impact of the finite model levels, limited horizontal resolution (approximately $1^{\circ}/1^{\circ}$ in the tropics) and temporal resolution (of 6 hours) on the model temperature field has been provided by Fueglistaler *et al.* [2005]. The focus here is on interannual variability, and we therefore assess the reliability of ERA-40 for this specific task by comparing time series of monthly mean temperatures of ERA-40 against alternative data sets.

[14] In general (see Appendix A), we find that ERA-40 tropical tropopause temperatures agree very well with radiosonde temperature data, in agreement with previous analyses [Simmons, 2003]. In particular, in agreement with Randel *et al.* [2004] we find that ERA-40 captures the cold temperatures much better than NCEP reanalyses. However, we find an obvious cold bias of the ERA-40 data with respect to radiosondes at the tropical tropopause for the

period 1979–1985 of about 1–2 K, and a weaker cold bias of order 1 K during 1986–1987. Further, the comparison presented by *Randel et al.* [2004] suggests a small warm bias of order 0.5 K in 1991 and 1993–1994.

3. Observations and Model Predictions of $[\text{H}_2\text{O}]_e$ and $[\text{H}_2\text{O}]_{T400}$

[15] In this section we will compare the model predictions to available measurements, quantify how well the model predictions reproduce the observations, and discuss the degree to which available observations can constrain model results.

[16] Figure 1 shows the monthly mean water vapor mixing ratios in the tropics (30°S to 30°N) at 400 K potential temperature $[\text{H}_2\text{O}]_{T400}$ and $[\text{H}_2\text{O}]_e$ of the model predictions (Figure 1a), and comparisons of the model predictions for $[\text{H}_2\text{O}]_{T400}$ with observations by HALOE (Figure 1b) and SAGE II and MLS (Figure 1c).

[17] Figure 1 shows that model predictions and observations are broadly in agreement over the entire period, and agree very well from about 1995 onward. Unfortunately, the ERA-40 data end in August 2002, and we refrain from presenting additional calculations (e.g., based on operational analysis data), so as not to introduce additional complications resulting from using different analyses. We note, however, that the dryness seen in 2003 and particularly in 2004 is accompanied by low temperatures, and there is little reason to doubt that the model calculations based on ERA-40 data, if it were extended to 2004, would capture also these observations.

[18] Obviously, the strong annual cycle renders a detailed assessment of the model skill difficult, and we thus will focus in the following discussion mostly on interannual anomalies (anomaly quantities will be identified with an asterisk, e.g., $[\text{H}_2\text{O}]_e^*$), which are obtained by subtracting a mean annual cycle from the time series shown in Figure 1.

[19] Figure 2 summarizes the results of our calculations of water vapor anomalies from SAGE II and HALOE measurements (Figure 2a; the limited duration of 19 months of the MLS measurements renders these data not suited for an analysis of interannual anomalies), and the results of the model calculations (Figures 1a, 2c, and 2d). In addition, (Eulerian) temperature anomaly fields of ERA-40 data (Figures 2b–2d) are shown that provide the context to discuss the results.

[20] Figure 2a shows that the predicted $[\text{H}_2\text{O}]_{T400}$ anomalies are generally in good agreement with observations. In particular, major anomalies on timescales of a few months or more are well reproduced. We note occasionally substantial differences on short timescales of a month, both between measurements by HALOE and SAGE II, as well as between measurements and model calculations. The low sampling frequency of the solar occultation instruments limits the accuracy to which we can determine monthly mean water vapor mixing ratios, which in turn limits the conclusions that can be drawn with respect to model accuracy on short timescales. We note, however, that the variability of all three signals is similar, and that often the short-term trend of all signals has the same sign, but differs in amplitude.

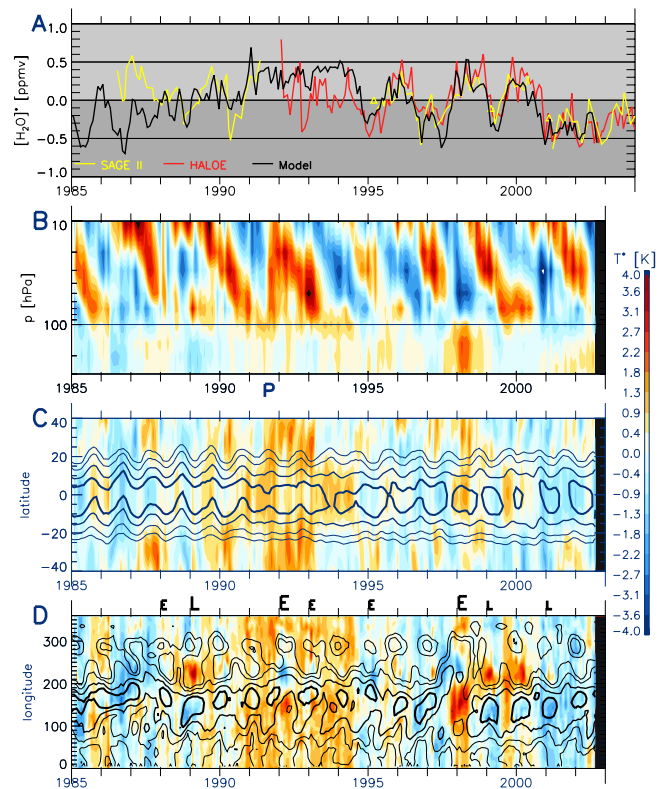


Figure 2. Interannual variability in tropical lower stratospheric water vapor and temperatures. (a) Lower stratospheric (at 400 K potential temperature) tropical (30°S to 30°N) monthly mean water vapor mixing ratio ($[\text{H}_2\text{O}]_{T400}$) anomalies. Yellow, SAGE II; red, HALOE; black, model predictions. (b) Anomalies of tropical (10°S to 10°N) monthly zonal mean ERA-40 temperatures. (c) Latitudinally resolved anomalies of zonal monthly mean ERA-40 temperatures at 100 hPa. Contour lines show latitudinal density of the Lagrangian cold points (contours indicate 0.5%/degree, 1%/degree, 2%/degree and 3%/degree). (d) Zonally resolved anomalies of tropical (10°S to 10°N) monthly mean ERA-40 temperatures at 100 hPa. Contour lines show zonal density of the trajectories' Lagrangian cold point (contours indicate 0.15%/degree, 0.25%/degree, 0.45%/degree and 0.7%/degree). Letters “E” and “L” refer to El Niño and La Niña events; larger letters indicate strong events. “P” refers to the eruption of Mount Pinatubo.

[21] On the basis of availability of observations, we may separate the further discussion into three periods.

3.1. Period From 1986 to 1991

[22] For this period only SAGE II observations are available, and the agreement with model predictions is only moderate. The SAGE II water vapor v6.2 employs a correction from January 1986 onward for a shift in the spectral response of the primary water vapor channel [*Thomason et al.*, 2004]. The application of an instantaneous, constant correction to compensate for a drifting channel could produce a spurious drift in the retrieved water vapor mixing ratio in the first years after the correction (i.e., the correction initially overcompensates the chan-

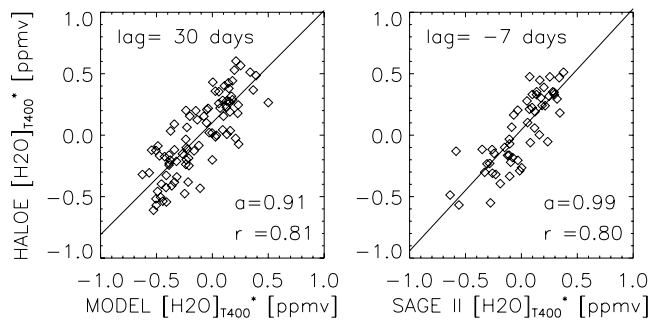


Figure 3. Scatterplot of (left) HALOE water vapor anomalies and model anomalies and (right) HALOE and SAGE II for 1995–2002, in the tropics at 400 K for lag (as indicated in figure) with maximum correlation. The slope of the linear regression is denoted as a , and the correlation coefficient is denoted as r .

nel drift). This would yield a moist bias, with a drift of order 1 ppmv for the period 1986 ~ 1988 (L. Thomason, personal communication, 2005). Further, the eruption of the volcano Nevado del Ruiz ($5^{\circ}\text{N}/75^{\circ}\text{W}$) in 1985 affects the data quality of the SAGE II water vapor in that period, and the dry spike seen in 1990 is most likely an artefact of the enhanced aerosol loading following the eruption of Mount Kelut ($18^{\circ}\text{S}/112^{\circ}\text{E}$) in February 1990 (L. Thomason, personal communication, 2005). The discrepancies between model predictions and SAGE II measurements during that period thus are likely due to an unfortunate combination of biases both in the SAGE II water vapor observations and in the ERA-40 temperature field, particularly in the period 1986–1987 (as previously discussed, see also Appendix A) underlying the model calculations. We note that the sign of the separation between the SAGE II observations and the model predictions before 1988 is consistent with a cold temperature bias affecting the model predictions, but the combination of biases in both time series prevents further conclusions for this period.

3.2. Period From 1992 to 1994

[23] The eruption of Mount Pinatubo in June 1991 prevents the use of SAGE II until 1995, and likely affects the HALOE observations in the months directly following the eruption. The MLS measurements shown in Figure 1, which are not affected by the volcanic aerosol, lend some credit to the HALOE measurements also during that period except for the large moist anomaly during the very first months of HALOE data. The SAGE II measurements seem to confirm an increase in water vapor during 1990–1991 compared to the period 1988–1990. The model calculations then predict a persistent moist anomaly of about 0.4 ppmv until early 1994. Such a persistent moist anomaly is not seen in the HALOE observations. The previously noted results of Randel *et al.* [2004] suggest a small warm bias of ERA-40 for the periods 1991 and 1993–1994, but its amplitude (about 0.5 K, corresponding to a moist anomaly of about 0.25 ppmv, see Figure 4b below) appears to be too small to fully account for the difference between the model predictions and HALOE observations. In summary, differences during this period, particularly during 1993–1994, cannot

unambiguously attributed to errors in either HALOE water vapor measurement or ERA-40 temperatures.

3.3. Period From 1995 to 2002

[24] Figure 2a shows that during this period model predictions agree very well with measurements, and HALOE and SAGE II observations are consistent over periods of a few months and more. The correlations between the HALOE and SAGE II on the one hand, and HALOE and model predictions on the other hand, are shown in Figure 3. Consistent with the phase lag of one month of the annual cycle due to overestimated vertical ascent in the lower stratosphere as discussed by Fueglistaler *et al.* [2005], the interannual anomalies of model predictions and HALOE show highest correlation when shifted by 30 days. Best agreement between HALOE and SAGE II anomalies is obtained at a lag of 7 days (Figure 3, right panel), with correlation coefficient $r = 0.8$. The correlation between model calculations and HALOE ($r = 0.81$) is thus as high as that between the two measurements ($r = 0.8$). In other words, the model predictions for the period 1995–2002 reproduce the observed water vapor mixing ratios to within measurement uncertainties.

3.4. $[\text{H}_2\text{O}]_e$ and the Lagrangian Cold Point Temperature

[25] In the following we will often discuss interannual variability in terms of temperature rather than water vapor mixing ratio. Figure 4a shows the monthly mean Lagrangian cold point temperature versus the corresponding mean water vapor mixing ratio (which includes the pressure dependence of the saturation mixing ratio), and Figure 4b shows their anomalies after subtracting the annual cycle. The annual cycle of the Lagrangian cold point pressure is similar to that of the tropical cold point tropopause, which is highest (and coldest) during boreal winter. The relation of the anomalies depends on the reference temperature and pressure, but Figure 4b shows that as a general rule a

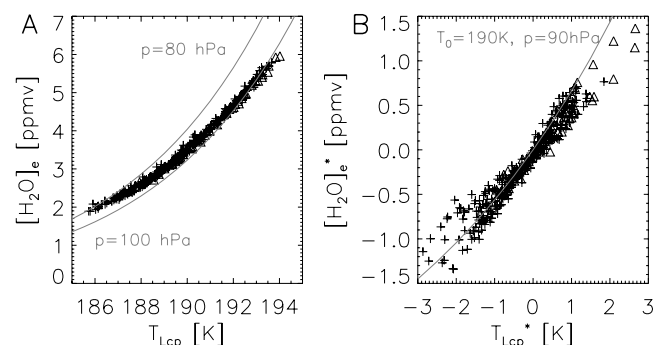


Figure 4. Monthly mean Lagrangian cold point temperatures and saturation mixing ratios for the period 1979–2002 (triangles for the period 1960–1964, see text). (a) Absolute values, and saturation mixing ratios at $p = 80$ and 100 hPa for reference. (b) Interannual anomalies after subtracting mean annual cycle (of the period 1990–2002). Grey curve is saturation mixing ratio anomaly for temperature anomalies from reference temperature 190 K and constant pressure 90 hPa.

Lagrangian temperature anomaly of 1 K corresponds to a water vapor entry mixing ratio anomaly of about 0.5 ppmv.

4. Processes Controlling Interannual Variability of $[\text{H}_2\text{O}]_e$

[26] The comparison of model calculations and observations in the previous section showed that the model calculations essentially capture the observed variability, and we are therefore interested in identifying the main processes that govern the interannual variability in the model calculations.

4.1. Quasi-biennial Oscillation

[27] The pattern of interannual variability in temperature shown in Figure 2b is dominated by characteristic downward phase propagation associated with the QBO [Baldwin *et al.*, 2001, and references therein]. While the QBO temperature signal is largest and most coherent above 100 hPa, a significant part of the signal penetrates to tropopause level, where it is associated with peak-to-peak variation in temperature of about 1 K. It has already been noted by Giorgetta and Bengtsson [1999], Geller *et al.* [2002], and others that this implies a variation in the water vapor mixing ratios entering the stratosphere. In our calculations the temperature anomalies associated with the QBO translate to anomalies in $[\text{H}_2\text{O}]_e$ of $\lesssim 1$ ppmv (as shown in Figure 4b). These in turn lead to anomalies of $\lesssim 0.5$ ppmv in $[\text{H}_2\text{O}]_{T400}$ (due to attenuation of the anomalies by lateral transport of extratropical air into the tropics), in good agreement with observations (Figure 2a).

[28] Figure 2c shows the latitudinally resolved zonal mean temperature anomalies at 100 hPa and the latitudinal density distribution of the Lagrangian cold point. The temperature anomalies associated with the QBO show a coherent structure with a width of about 30° in latitude, centered at the equator, in agreement with the estimate of the latitudinal scale $L \approx 1000\text{--}1200$ km by Randel *et al.* [1999]. The latitudinal density distribution of the Lagrangian cold point shows a north-south oscillation over the course of the year, with the northward shift during boreal summer being a result of the Indian/Southeast Asian monsoon circulation (see also Figure 5 of Fueglistaler *et al.* [2005] for seasonal maps of the density distribution of the Lagrangian cold points). Despite this latitudinal oscillation, the Lagrangian cold point distribution is largely confined to the inner tropics, and thus coherently and strongly affected by QBO-induced temperature perturbations.

[29] The temperature variation is much more irregular at the tropopause (i.e., near 100 hPa) than at, say, 50 hPa and above. There is well-known irregularity in the QBO signal in the lower stratosphere, associated with “stalling” of the descent of the easterlies and unusually persistent westerlies below [e.g., Kinnerson and Pawson, 1996], and the irregularity in the temperature signal has similar character. One description of this irregularity is that the downward propagation associated with the changing phase of the QBO does not, on occasion, continue all the way to the tropopause. For example, the temperature pattern above 50 hPa suggests that boreal winter 1991/1992 should be cold, but the downward propagation of the cold anomaly stops mid-1991 at about 80 hPa. This may be at least partly due to the

effects of the Pinatubo eruption. Indeed, the extended cold period from 2000 onward may be described as resulting from the fact that the QBO warm anomaly expected in late 2002 failed to propagate down to 100 hPa.

4.2. El Niño–Southern Oscillation

[30] The El Niño–Southern Oscillation (ENSO) has a profound impact on the distribution of convection over the Pacific and, correspondingly, the temperature field and circulation around the tropical tropopause also experience profound changes.

[31] Figure 2d shows the longitudinally variation of tropical temperature anomalies. During the El Niño phases (marked with “E”), the western Pacific 100 hPa level shows a warm anomaly, and the eastern Pacific a cold anomaly. During the La Niña phases, these anomalies are inverted. The zonal density distribution of the Lagrangian cold point (Figure 2d, contour lines) shows that during El Niño, the density distribution is substantially shifted eastward, as already noted by Bonazzola and Haynes [2004]. This shift away from the strong warm anomaly over the western Pacific greatly reduces its potential impact on $[\text{H}_2\text{O}]_e$. The net effect of El Niño/La Niña situations on $[\text{H}_2\text{O}]_e$ is, during the period shown in Figure 2, often not clearly discernible, and their impact on zonal mean tropical tropopause temperatures is in general weak (Figure 2b), as previously noted by Gettelman *et al.* [2001]. Generally, we find that at least strong El Niño situations have a moistening impact (of order a few tenths of a ppmv over a period of several months) on $[\text{H}_2\text{O}]_e$, and La Niña situations, if anything, a drying impact, in agreement with the AGCM simulations reported by Gettelman *et al.* [2001], Hatsushika and Yamazaki [2003], and Scaife *et al.* [2003]. Certainly, the exceptionally strong El Niño in 1997/1998 is associated with a clear warm anomaly (note the coincidence with the QBO warm phase which, however, does not reach the tropopause) in zonal mean 100 hPa temperatures, and the model calculations show that this warming is also reflected in the mean Lagrangian cold point and hence leads to an increase in $[\text{H}_2\text{O}]_e$ in that period. On the other hand, the strong La Niña situation in 1988/1989 is associated with a short dry anomaly at the end of 1988 in agreement with the SAGE II measurement (Figure 2a), but the sequence of temperature fluctuations in the lower stratosphere during that period (Figure 2b) make it difficult to determine how much of the dry signal is a result of the La Niña situation and how much is caused by other processes affecting tropopause temperatures.

4.3. Eruption of Mount Pinatubo

[32] Strong volcanic eruptions in the tropics can inject large amounts of aerosol into the lower stratosphere, which in turn leads to a warming of that region [e.g., Bluth *et al.*, 1992; Kinnison *et al.*, 1994] and hence potentially to a moistening of the stratosphere. The most notable eruption during the period shown here was that of Mount Pinatubo in June 1991, and the resulting warming is clearly seen in the ERA-40 data (Figure 2b, indicated with “P”). The ERA-40 temperature data at the tropical tropopause suggest that a warm anomaly associated with the QBO preceded the Pinatubo-induced warming, and the strong El Niño situation in the following year (1991/1992) also lead to a warming,

such that the Pinatubo-induced warming is embedded in warm anomalies. This coincidence of a sequence of warm anomalies explains why the predicted $[\text{H}_2\text{O}]_e$ does not show any particular increase after the eruption.

[33] As already noted, the agreement of the model calculations with HALOE in the three years following the eruption is poor and it may be that this results from an unusually large role for processes neglected in the model, e.g., an unusual effect of the large aerosol loading on microphysical processes.

5. Lagrangian Cold Point and Eulerian Mean Tropical Tropopause Temperatures

[34] The conclusion of *Fueglistaler et al.* [2005], reiterated here, is that absolute values of water vapor mixing ratios in the stratosphere, including annual variation, are determined by the Lagrangian cold point distribution, and are poorly predicted by any Eulerian mean measures of tropical temperatures. The question we examine here is whether the same is true for year-to-year variations in water vapor mixing ratios.

[35] The spatial density distribution of the Lagrangian cold point as shown in Figures 2c and 2d shows substantial interannual variability, and it may be that the interannual variability of localized processes (e.g., of the Indian/Southeast Asian monsoon circulation, or ENSO) modulate $[\text{H}_2\text{O}]_e$ more strongly than the variability of the zonal mean state, with important implications for the interpretation of long-term trends of stratospheric water vapor in section 7 below.

[36] The Eulerian proxy employed here is the tropical mean 100 hPa temperature (denoted as T_{100} for the zonal average from 10°S to 10°N). Figure 5 shows the time series of the anomalies of the Lagrangian cold point T_{Lcp}^* and the monthly mean tropical 100 hPa temperature T_{100}^* . Here we discuss the results for the period 1979–2002 (the period 1960–1964 will be discussed later in section 7.1).

[37] The two time series are highly correlated (with $r = 0.87$) on all timescales, with a few notable exceptions, when the Lagrangian cold point temperature anomaly is clearly colder than the corresponding T_{100}^* (most notable in 1980, 1985, 1986, 1998/1999 and 2001/2002), with a prevalence for larger deviations during boreal winter.

[38] When comparing water vapor anomalies predicted from T_{100} directly to HALOE observations over the period 1995–2002, we find high correlations (with $r = 0.69$ and $r = 0.7$, depending on the details of the method to derive water vapor anomalies from T_{100} ; data not shown), similar to that presented by *Randel et al.* [2004] ($r = 0.72$) using radio-sonde tropical cold point temperatures.

[39] Thus the Lagrangian calculations (with $r = 0.81$) are an improvement to predictions based on tropical mean 100 hPa temperatures, and in particular provide the physical explanation for the observed correlations. However, the fact that the Lagrangian cold point is highly correlated to T_{100} suggests that most of the variability of $[\text{H}_2\text{O}]_e$ is explained by zonal mean temperature anomalies. In other words, we find that it is the superimposed temperature variation, as represented by the zonal mean (see Figure 2b), that determines most of the variation in $[\text{H}_2\text{O}]_e$, rather than variation in the location of the Lagrangian cold points or localized temperature trends (see Figures 2c and 2d).

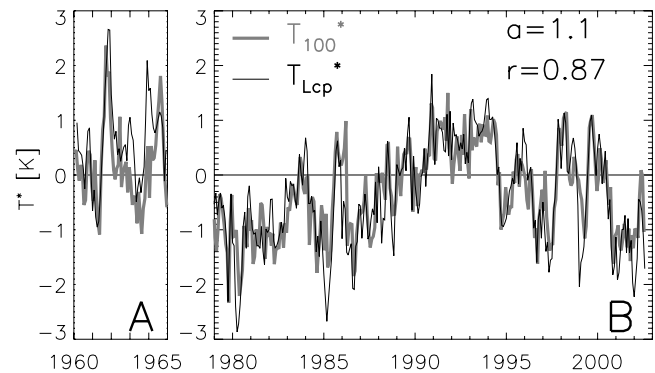


Figure 5. Temperature anomalies of the mean Lagrangian cold point (T_{Lcp}^*) and tropical (10°S to 10°N) monthly mean temperatures at 100 hPa (T_{100}^*) for the periods (a) 1960–1965 and (b) 1979–2002. The slope of the linear regression is denoted as a , and the correlation coefficient is denoted as r (for the period 1979–2002). Anomalies were calculated by subtracting the mean annual cycles of the period 1990–2002. Note that ERA-40 absolute temperatures seem to be higher in the 1960–1965 period, but what we are emphasizing here is not absolute values, but the correlation between T_{Lcp}^* and T_{100}^* .

[40] Finally, we note a change in the annual north-south oscillation of the latitudinal density distribution of the Lagrangian cold point from about 1991 onward (Figure 2c), accompanied by a slight broadening of this distribution. This might have been indicative of a broadening of the tropical upwelling, which has been hypothesized to be a possible mechanism for long-term stratospheric water vapor trends [*Zhou et al.*, 2001; *Rosenlof*, 2002]. A closer inspection shows that in fact the region of coldest temperatures around the tropopause is broadening, which in turn induces the change seen in the latitudinal Lagrangian cold point distribution. However, this change has little net effect on $[\text{H}_2\text{O}]_e$.

6. Water Vapor in the Midlatitude Stratospheric Overworld

[41] The longest continuous time series of stratospheric water vapor have been measured by balloon-borne chilled-mirror hygrometers over the northern hemisphere midlatitudes, from 1964 to 1977 over Washington, D. C., and since 1980 over Boulder, Colorado [*Oltmans et al.*, 2000].

[42] These unique observations provide most of the available information of past stratospheric water vapor concentrations, in particular those of the stratospheric overworld, and hence are an essential point of reference for multidecadal variability. In this section we relate our model predictions for $[\text{H}_2\text{O}]_e$ over the period 1979–2002 to measurements over Boulder, Colorado, by the NOAA Climate Monitoring and Diagnostics Laboratory (CMDL) and spaceborne observations from the time when they become available. To ensure that observations represent stratospherically older air (and hence to minimize spurious variation in the model results due to incorrect representation of outflow of stratospherically young air from the tropics in the lower stratosphere), we compare observations and

model predictions at a potential temperature of 600 K (about 24 km altitude).

[43] The effects of stratospheric transport and chemistry complicate the interpretation of observations in the midlatitude stratospheric overworld with respect to $[\text{H}_2\text{O}]_e$. The approach taken here is using a simple model for stratospheric transport, where we account for stratospheric transport from the tropics to the midlatitudes by convolving $[\text{H}_2\text{O}]_e$ with an appropriate age spectrum, and a weighting of the monthly mean mixing ratios with the seasonally varying mass flux across the tropical tropopause. The effect of chemistry, namely methane oxidation, is evaluated as follows. Total hydrogen is conserved in the stratospheric overworld, and is to a very good approximation the sum of the concentrations of molecular hydrogen, water vapor and methane: $[\text{H}] \equiv [\text{H}_2] + [\text{H}_2\text{O}] + 2 \times [\text{CH}_4]$, and from measurements it is known that molecular hydrogen concentrations are very constant throughout the stratosphere [e.g., Zöger *et al.*, 1999]. We therefore consider only water vapor and methane. As our focus is on $[\text{H}_2\text{O}]_e$ rather than on the contribution from methane oxidation ($[\text{H}_2\text{O}]_{\text{CH}_4}$), and its interannual variation due to changes in stratospheric transport and chemistry, we will encapsulate all processes governing methane oxidation in a single parameter γ . That is,

$$[\text{H}_2\text{O}]_{\text{CH}_4}(t) \equiv [\text{CH}_4]_e(t - \bar{\tau}) \cdot \gamma(t)$$

where the methane mixing ratio at entry into the stratosphere $[\text{CH}_4]_e$ is set to the tropospheric methane mixing ratio (taken from the data presented by Dlugokencky *et al.* [1998] and Etheridge *et al.* [1992]), and $\bar{\tau}$ is the mean stratospheric age. The use of the mean stratospheric age instead of fully accounting for the stratospheric age spectrum is justified by the fact that interannual anomalies of tropospheric methane concentrations are much smaller than its average value. The fraction γ (with units of concentration of water vapor divided by concentration of methane) then is

$$\gamma(t) = \alpha \cdot (1 - \beta(t)), \quad (4)$$

$$\beta(t) \equiv \frac{[\text{CH}_4](t)}{[\text{CH}_4]_e(t - \bar{\tau})} \quad (5)$$

where β is the fraction of retained methane, $[\text{CH}_4]$ is the stratospheric methane concentration at a given latitude and height, and $\alpha \approx 2$ [Le Texier *et al.*, 1988]. We calculate β for the stratospheric overworld over Boulder, Colorado, from methane measurements by HALOE at 600 K potential temperature within 2° latitude and 15° longitude of Boulder, Colorado. Figure 6 shows that in the 1990s $\beta = 0.67 \pm 0.05$ with a negligible linear trend of 0.008/decade. We therefore neglect the time dependence of β and γ .

[44] We may then write the water vapor mixing ratio in the midlatitude stratospheric overworld ($[\text{H}_2\text{O}]_o$) as

$$[\text{H}_2\text{O}]_o(t) = \int_0^6 [\text{H}_2\text{O}]_e(t - \tau) \cdot w(t - \tau) \cdot h(\tau) d\tau + [\text{CH}_4]_e(t - \bar{\tau}) \cdot \gamma \quad (6)$$

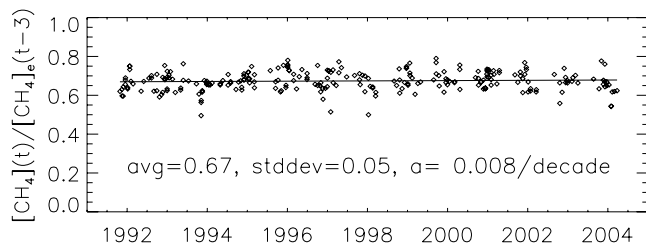


Figure 6. Fraction of retained methane $\beta(t)$ for Boulder, Colorado, at 600 K potential temperature determined from HALOE methane mixing ratios ($[\text{CH}_4]$) and methane mixing ratios at entry into the stratosphere ($[\text{CH}_4]_e$) shifted by 3 years to account for mean stratospheric age.

where the seasonal weighting $w(t)$ of TST is taken from Holton [1990] and the (climatological mean) stratospheric age spectrum $h(\tau)$ from Waugh and Hall [2002], and truncated at 6 years (the conclusions drawn below are not sensitive to the precise shape of the age spectrum).

[45] Figure 7a shows the previously discussed results of the model predictions for $[\text{H}_2\text{O}]_e^*$, and the increase $\Delta[\text{H}_2\text{O}]_e$ estimated from the ATMOS measurements (subtracting the ATMOS estimate for $[\text{H}_2\text{O}]_e$ of the 1985 mission from that of the later missions). Both model and measurement indicate an increase from the early to middle 1980s to the early 1990s, with the model predictions of $\Delta[\text{H}_2\text{O}]_e \approx 0.7$ ppmv being larger than the $\Delta[\text{H}_2\text{O}]_e \approx 0.3$ ppmv of the ATMOS data [see also Fueglistaler *et al.*, 2005].

[46] Figure 7b shows the model predictions based on equation (6) for the stratospheric overworld over Boulder at 600 K, with the contributions from $[\text{H}_2\text{O}]_e$ and methane oxidation indicated. The model predictions start in 1985 because of the convolution of $[\text{H}_2\text{O}]_e$ (starting in 1979) with an age spectrum of 6 years. The range of uncertainty (black bars) is given by the standard deviation of the fraction of retained methane (β , see equation (5)).

[47] Figures 7c–7e compare the model predictions to measurements by the CMDL frost point hygrometer, HALOE and SAGE II measurements (located within 2° latitude and 15° longitude of Boulder). In addition to the individual measurements a running mean averaging 12 months of data (solid line), and the corresponding standard deviation (grey bars), is shown. The model prediction and (running mean) measurements are again summarized in Figure 7f.

[48] The model predictions are generally in good agreement with all three observations, despite their neglect of variability of stratospheric transport and chemistry. The variability within a 12 month period, as well as interannual variability, is smallest in the HALOE observations. The interannual variabilities seen in the CMDL and SAGE II observations are often not consistent. For example, the high values observed in 1994 by SAGE II are likely an artefact of the aerosol contamination following the Pinatubo eruption. Also, over the period 1986–1988 the SAGE II observations are moister than the CMDL observations and model predictions, which supports the previously expressed view that SAGE II water vapor in that period suffers from an artificial trend due to a correction applied at the beginning of 1986.

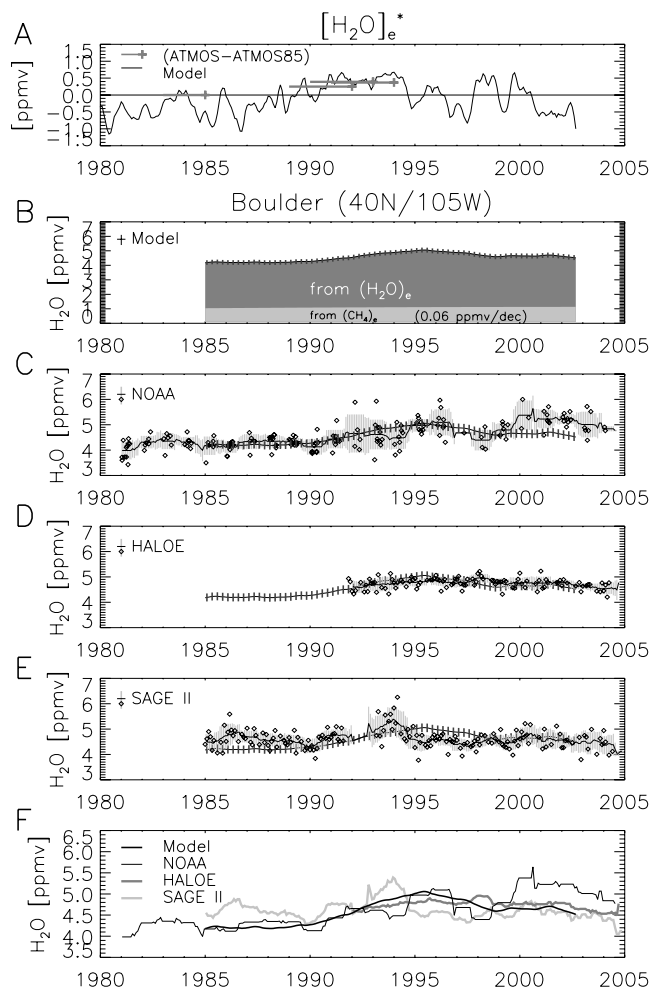


Figure 7. (a) Anomalies of entry values of water vapor from model calculations, and ATMOS measurements [Michelsen *et al.*, 2000] relative to the value inferred for the 1985 mission (bars of length 3 years indicate approximate period of entry into stratosphere). (b) Model predictions for Boulder, Colorado, at a potential temperature of 600 K (24 km altitude) based on model calculation for $[\text{H}_2\text{O}]_e$ and a simple model for stratospheric transport and chemistry (see text). Uncertainty shown is ± 1 standard deviation of ratio of oxidized methane. (c) NOAA frost point measurements at 600 K (line shows running mean over 12 months' measurements; uncertainty (light grey) is ± 1 standard deviation) and the model predictions. (d) Same as Figure 7c, but for HALOE measurements. (e) Same as Figure 7c, but for SAGE II measurements. (f) Summary for model predictions and available observational data. Note that the model predictions prior to the 1990s are affected by biases in ERA-40 temperatures (see text).

[49] The CMDL data suggest that water vapor mixing ratios were fairly constant throughout the 1980s, with an increase in the early/mid 1990s and another around 2000. The latter is not seen in either of the spaceborne observations, and also not in the model predictions, which are considered to be very reliable for this period (recall the

previous discussion of $[\text{H}_2\text{O}]_e$ for the period 1995–2002). The CMDL data show at times a pronounced altitude-dependent variability on timescales of a few years (not shown; for example, following the high values around the year 2000, altitudes below about 23 km show a more rapid decrease of water vapor mixing ratios than at 24 km [see, e.g., Randel *et al.*, 2004, Figure 8]). The differences among the measurements of different instruments highlight on the one hand the difficulty of tightly constraining model calculations, and on the other hand the difficulty of deriving reliable trends from observations (depending on the time window, very different linear trends may be obtained from the 3 observational time series). The trend differences between HALOE and CMDL frost point hygrometer measurements are also discussed by Randel *et al.* [2004].

[50] As it turns out the linear trend over the period 1985–2000 calculated from the model (0.55 ppmv/decade, of which 0.06 ppmv/decade result from increasing tropospheric methane concentrations) is almost identical to that of the CMDL observations (0.57 ppmv/decade). However, given the previously discussed cold biases of ERA-40 in the 1980s this agreement must be regarded as largely fortuitous. Without the bias in the ERA-40 temperature data the model-predicted trend would be significantly smaller, and perhaps closer to the ATMOS observations.

[51] Despite the simplicity of the model used above (assuming constant methane oxidation and age spectrum), the predictions for midlatitude stratospheric water vapor agree rather well with observations. The disagreements that are seen between model predictions and observations are similar in magnitude to differences seen between different instruments. In particular there is therefore no ground for arguing that the prediction of $[\text{H}_2\text{O}]_e$ by the model, or its representation of stratospheric transport and chemistry, are inadequate.

7. Long-Term Trends of Stratospheric Water Vapor

[52] The extensive comparison of model predictions and observations presented in sections 3 and 6 showed that the model predictions are able to reproduce observed variability of stratospheric water vapor on interannual to decadal scale to within observation uncertainty, leaving only a small margin for undetected systematic trends in the residuals. This strongly suggests that the model calculations based on ERA-40 wind and temperature fields capture the main processes controlling $[\text{H}_2\text{O}]_e$. Referring to equations (1) and (2), implications consistent with our results are as follows: (1) $f_1 \cdot \chi_1 \gg f_2 \cdot \chi_2$ and (2) the assumption $\epsilon \ll \min(\chi^{\text{sat}}(T_{\text{syn}}))$, $\epsilon \approx \text{constant}$ is well justified, at least under present-day conditions (except possibly for the post-Pinatubo period). In other words, the implicit assumptions in the model calculations are justified by their agreement with observations. Further, the comparisons in the midlatitude stratospheric overworld at a potential temperature of 600 K (section 6) did not reveal any need to take account of changes in stratospheric transport or chemistry to explain observed water vapor concentrations to within observational uncertainties; that is, they are consistent with the following assumption: (3) $\gamma \approx \text{constant}$ over time for the past two decades.

[53] The question we address here is whether the identified processes controlling $[\text{H}_2\text{O}]_e$ are sufficient to explain water vapor variations in the stratospheric overworld on multidecadal scales, or whether additional processes are required, and whether this would be consistent with implications 1–3 above. Note that the discussion is restricted to the overworld as we do not model extratropical troposphere-stratosphere exchange processes.

[54] An analysis of long-term trends of stratospheric water vapor, and their causes, is confronted with two severe difficulties. First, the reanalysis data prior to 1979 are based on radiosonde observations only, and the inclusion of satellite based observations from 1979 onward could induce spurious trends in the model calculations. Second, the water vapor observations in the stratospheric overworld prior to the 1980s are extremely sparse, and essentially limited to the Naval Research Laboratory (NRL) measurements with balloon-borne frost point hygrometers (for an overview of available observations see *Rosenlof et al.* [2001]). The interpretation of these data with respect to $[\text{H}_2\text{O}]_e$ is further hampered by the lack of simultaneous and colocated methane measurements.

[55] We therefore proceed as follows. Instead of searching for indications of long-term trends in the comparisons shown in the previous sections, we take the proposed long-term trend as published by *Rosenlof et al.* [2001] and deduce the implications for $[\text{H}_2\text{O}]_e$ in the 1960s.

7.1. Observed Long-Term Trends and Implications for $[\text{H}_2\text{O}]_e$

[56] *Oltmans et al.* [2000] report a trend of 0.79 ± 0.48 ppmv/decade for the period 1964–1977 and 0.44 ± 0.12 ppmv/decade for the period 1980–2000. The combined trends, and assuming that the discontinuity between the two time series is due to a bias of the 1964–1977 NRL measurements, yield a continuous increase of on average 1%/year, or about a doubling of stratospheric water vapor over the past 4 decades [*Rosenlof et al.*, 2001].

[57] Figure 8 reproduces the water vapor observations over Washington, D. C., and Boulder, Colorado, and the linear trends (as shown by *Oltmans et al.* [2000, Figures 1 and 3], and the data interpretation of *Rosenlof et al.* [2001] (shaded). Assuming present-day, constant γ (see equation (4)) and historic tropospheric methane concentrations as provided by *Dlugokencky et al.* [1998] and *Etheridge et al.* [1992], the figure further shows an estimate for $[\text{H}_2\text{O}]_e$ (dark grey shaded).

[58] The implication of this is that around 1960, $[\text{H}_2\text{O}]_e$ was about 1.5 ppmv assuming stratospheric transport and chemistry controlling methane oxidation (as encapsulated by γ) was similar to today. Even if we assume dramatic changes in γ such that methane oxidation did not contribute to midlatitude stratospheric water vapor, $[\text{H}_2\text{O}]_e$ would still have to be around 2.5 ppmv in the 1960s. Thus $[\text{H}_2\text{O}]_e$ would have been 1–2 ppmv drier than today, which implies, assuming similar circulation as today, about 2–4 K lower temperatures around the tropical tropopause (see Figure 4b). Although the amplitude of such a change in temperature is not impossible a priori, published observational evidence points, if anything, to slightly higher, rather than lower, tropical tropopause temperatures in past decades. *Seidel et al.* [2001] report a negative trend of about 0.5 K/decade for

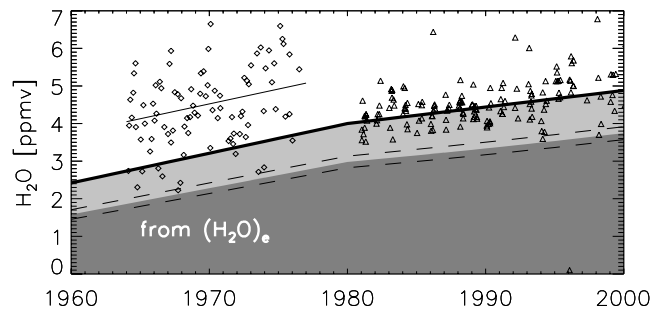


Figure 8. Implications of long-term trends observed at Boulder, Colorado, on $[\text{H}_2\text{O}]_e$ (dark grey) if trends are taken at face value, and assuming that instrumental bias between Washington, D. C., series (1964–1977, diamonds) and Boulder, Colorado, series (1977–1997, triangles) is entirely a bias of the Washington, D. C., measurements. Linear trends and data points are taken as published by *Oltmans et al.* [2000] for the altitude range 24–26 km, tropospheric methane is taken as published by *Dlugokencky et al.* [1998], and the retained methane fraction is determined from HALOE over the period 1992–2000 ($\beta = 0.67 \pm 0.05$, see text), with the contribution from oxidized methane shown in light grey. Dashed black lines show $[\text{H}_2\text{O}]_e$ when β is varied by 1 standard deviation.

the period 1978–1997, and *Zhou et al.* [2001] report a negative trend of 0.57 K/decade for the period 1973–1998. Most recently, *Lanzante et al.* [2003] estimate for temperatures at 100 hPa in the tropics a negative trend of 0.15 K/decade for the period 1959–1997 (significantly smaller in magnitude than the estimated trends over shorter and more recent periods, but still of the same sign).

[59] Explorative trajectory calculations of $[\text{H}_2\text{O}]_e$ for the period 1960–1964 based on ERA-40 data yield similar mean and variability of $[\text{H}_2\text{O}]_e$, and a similar relation between T_{Lcp}^* and $[\text{H}_2\text{O}]_e^*$ (see Figure 4), as observed for the period 1979–2002. Further, the high correlation between the Lagrangian cold point temperature anomalies T_{Lcp}^* and tropical mean 100 hPa temperature anomalies T_{100}^* persists also in the early 1960s (see Figure 5a). It follows that circulation changes or localized temperature effects on multidecadal timescales (rather than over the period 1979–2002) are unlikely to account for trends of order 1–2 ppmv/40 years in $[\text{H}_2\text{O}]_e$ relative to estimates based on zonal mean temperatures (i.e., T_{Lcp}^* (black) would have to be 2–4 K lower than T_{100}^* (grey) in the 1960s, which is not seen in the data shown in Figure 5a).

[60] It thus appears that either the long-term trend (and its implied dryness of the stratosphere in the 1960s) is due to a process not considered in the model calculations for $[\text{H}_2\text{O}]_e$, or that the long-term trend has been overestimated.

7.2. Potential Role of Neglected Processes

[61] Let us first consider the potential role of processes not taken into account in the model calculations. Recalling equation (1) and implication 1 above, a trend arising from unresolved tropical TST (i.e., F_2) can be large only if either the fraction f_2 was significantly larger in the past, or its associated mixing ratio has experienced a very strong trend (since $f_1 \cdot \chi_1 \gg f_2 \cdot \chi_2$, $d\chi_2/dt \gg 1$ ppmv/40 years is

required for $d[\text{H}_2\text{O}]_e/dt \approx 1$ ppmv/40 years). *Sherwood* [2002] suggested that increasing tropospheric aerosol concentrations (due to biomass burning) could affect the dehydration efficiency in overshooting convection, but did not provide a quantitative estimate of the resulting trend. The argument given above renders it doubtful whether such a mechanism could account for a trend of the required magnitude. Alternatively, one might speculate that the fraction of unresolved TST (f_2) was much larger in the past, but we are not aware of indications that tropical convection has undergone drastic changes since the 1960s.

[62] Finally, processes that affect the balance in ϵ (equation (2)) in principle could strongly affect $[\text{H}_2\text{O}]_e$ because they act on the dominant mass flux F_1 . *Notholt et al.* [2005] explored the possibility that increasing SO_2 emissions in southern and eastern Asia could have affected particle number density of tropical cirrus clouds, and hence their dehydration efficiency. However, their model calculations suggest a positive trend of at most 0.5 ppmv/50 years.

[63] In summary, neither the model calculations reflecting synoptic-scale transport and temperatures, nor trends in processes not considered in the model calculations, seem likely to be able to explain a trend of the magnitude proposed by *Rosenlof et al.* [2001]. We therefore feel that it is justified to reconsider their data interpretation. In particular, we are concerned about the following aspects.

7.3. Has the Long-Term Trend Been Overestimated?

[64] The suggested trend is based on two time series of two different instruments that do not overlap (see *Oltmans et al.* [2000] for a discussion), and independent observations confirming the accuracy of the 1964–1977 time series do not exist. The conclusion of a large long-term trend critically hinges on the combination of the trends of the two time series and implicitly assumes that the 1964–1977 observations have a mean moist bias of about 1 ppmv (see Figure 8). We note that this time series shows a sequence of relatively high water vapor mixing ratios from 1972 to 1977 that have a strong impact on the linear trend calculation and on the bias between the two time series. Given the systematic differences between the CMDL and spaceborne observations from about 2000 onward (recall Figure 7) or the differences in linear trend estimates reported by *Randel et al.* [2004], it cannot be excluded that the NRL measurements are subject to similar uncertainties. In addition, the strong modulations of $[\text{H}_2\text{O}]_e$ on timescales of months to years induce variation at midlatitudes, whereby the slow stratospheric circulation (with mixing on various scales) acts as a low-pass filter. The resulting low-frequency variation of midlatitude water vapor concentrations implies that many years of continuous data may be required for a reliable analysis of long-term trends.

8. Summary and Conclusions

[65] In this paper we have further examined the Lagrangian calculations of troposphere-to-stratosphere transport, based on ERA-40 temperatures and winds, reported by *Fueglistaler et al.* [2005], with particular emphasis here on the interannual variability and systematic changes in stratospheric water vapor, and the processes governing $[\text{H}_2\text{O}]_e$. The main conclusions of this extensive comparison

of model predictions to available measurements by SAGE II, HALOE, MLS, ATMOS and the NOAA frost point hygrometers, of stratospheric water vapor are as follows.

[66] 1. The model calculations explain observed interannual variability in the tropical lower stratosphere to within measurement uncertainties during the period 1995–2002, where the temperature fields underlying our calculations are in good agreement with radiosondes, and measurements of water vapor are consistent among various sensors. This conclusion may be extended back to about 1986, if we accept that discrepancies between model predictions and observations during 1986–1994 are largely remedied when temperature biases and observation biases are taken into account (for which we have presented evidence). This compellingly demonstrates that at least up to decadal timescales the observed variability is controlled by synoptic-scale temperatures and dynamics of tropical TST. A corollary is that processes not resolved by ERA-40, such as individual convective cells penetrating the tropopause, may play only a secondary role for the stratospheric water vapor budget under present conditions.

[67] 2. Some of the variability is clearly associated with the QBO, which accounts for temperature anomalies of order 1 K near the tropical tropopause, leading to anomalies in $[\text{H}_2\text{O}]_e$ of order 0.5 ppmv. Part of the variability is more irregular, and it is not clear whether this is best interpreted as being associated with irregularities in the QBO itself, or as arising from some dynamical variability that is essentially independent of the QBO. In addition to the QBO, strong ENSO events lead to clearly attributable anomalies in stratospheric water vapor. ENSO events induce large changes in the circulation and temperature fields (leading to changes in the spatial density distribution of the Lagrangian cold points) over the Pacific, whereby the changes in circulation tend to attenuate the effect of changes of zonal temperature inhomogeneities on $[\text{H}_2\text{O}]_e$, leading to a net anomaly in $[\text{H}_2\text{O}]_e$ that resembles that of the tropical mean 100 hPa temperature field. In particular, the strong El Niño of 1997/1998 unambiguously leads to a moist anomaly of order 0.5 ppmv for several months. Together, QBO and ENSO modulate $[\text{H}_2\text{O}]_e$ with amplitudes of order 0.5 ppmv and periods of several months to years. The conclusions regarding the roles of the QBO and ENSO are consistent with those of previous authors, but the trajectory approach provides a more justifiable link between variability in temperatures (and circulation) and variability in water vapor.

[68] 3. Observations in the midlatitude stratospheric overworld at a potential temperature of 600 K by the NOAA CMDL frost point hygrometer, SAGE II and HALOE were compared with model calculations based on the predicted $[\text{H}_2\text{O}]_e$ and contributions from methane oxidation during transport from the tropics to the midlatitudes. Despite the extremely simplified treatment of stratospheric transport and chemistry (the fraction of methane oxidized to water was assumed to be constant over the entire period 1979–2002), the comparison showed reasonable agreement. Similar to the situation in the tropics, the differences between the measurements of different instruments did not allow strong conclusions on whether the model calculations miss essential aspects either in $[\text{H}_2\text{O}]_e$ or stratospheric transport and chemistry. A corollary is that apparently the latter do not

induce readily detectable interannual anomalies of water vapor in the midlatitude stratosphere.

[69] 4. The strong preference of the Lagrangian cold point for regions of coldest temperature is the reason for the lower observed mixing ratios than those expected from Eulerian mean temperature calculations [Fueglistaler *et al.*, 2005]. These (zonal) anomalies are therefore crucial for explaining observed concentrations of stratospheric water vapor. However, while we find that the interannual anomalies of tropical water vapor mixing ratios at 400 K are better correlated with the Lagrangian predictions ($r = 0.81$) than with anomalies of the tropical 100 hPa temperatures ($r = 0.7$), the difference is not very large. This appears to be due to the fact that a significant part of the interannual variability in temperatures near the tropical tropopause is zonally symmetric (recall Figure 2d). In other words, temperature anomalies of the zonal mean state dominate over anomalies due to localized temperature trends or circulation anomalies.

[70] 5. The conclusion of, in practice, a tight control of $[\text{H}_2\text{O}]_e$ by zonal mean temperature anomalies is at odds with suggested long-term trends of stratospheric water vapor corresponding to about a doubling of $[\text{H}_2\text{O}]_e$ since the 1960s [Rosenlof *et al.*, 2001]. ERA-40 temperatures in the tropics at 100 hPa (or cold-point tropopause temperatures from radiosondes [Seidel *et al.*, 2001; Zhou *et al.*, 2001]) do not show a positive trend of the required order (2–4 K over 4 decades) to account for the postulated water vapor trend, neither do exploratory trajectory calculations in the early 1960s indicate differences to those of the period 1979–2002 that could account for the suggested long-term trend.

[71] 6. The good agreement of model and observations on decadal timescales constrains potential trends in $[\text{H}_2\text{O}]_e$ due to processes not considered in the model calculations. We have discussed a range of suggested processes, but none seems to be able to produce trends of the required magnitude without having to invoke drastic changes of tropical dynamics since the 1960s. Alternatively, we have considered the possibility that long-term trends simply have been overestimated. We noted that the conclusion of substantial long-term trends critically hinges on the combination of linear trends in two nonoverlapping time series. Further, the extensive comparison of water vapor measurements reveals substantial differences among different instruments at times, which on the one hand limit our capability to strongly constrain model results, and on the other hand raise doubt as to whether past observations of stratospheric water vapor are accurate enough to provide reliable trend estimates. Moreover, the strong interannual variability of $[\text{H}_2\text{O}]_e$ of ± 0.5 ppmv over periods of months to years requires continuous observations, probably over several decades, to ensure that trend estimates truly reflect long-term changes.

[72] It is hoped that future reanalysis projects will provide data with less spurious temperature trends around the tropopause, such that the model calculations for the period before about 1985 will become more reliable. However, the water vapor data against which model results will have to be compared to remains the same, and it appears doubtful whether much more insight on the control of stratospheric water vapor may be obtained from those data. Rather, the continuation of present-day observations of temperature and water vapor mixing ratio relying on approved techniques as

well as on new sensors and techniques (e.g., GPS radio-occultation, or MLS on board the AURA satellite) will provide eventually a multisensor time series long enough to further constrain model results, and to quantify processes that affect $[\text{H}_2\text{O}]_e$ apart from the synoptic-scale temperatures and dynamics of tropical TST.

Appendix A: Accuracy of ERA-40 Temperatures

[73] Figure A1a shows the tropical mean 100 hPa temperatures of ERA-40 and NCEP reanalysis data [Kalnay *et al.*, 1996] for the period 1979–2002. The two reanalysis temperature series agree well from the late 1990s onward, and have a fairly constant offset of about 3 K back to the mid-1980s. In the early 1980s, however, the temperature difference is about 4 K as a result of a drop in temperatures in the ERA-40 data that is not observed in the NCEP data.

[74] Figure A1b shows the temperature anomalies after subtracting the annual cycle of the ERA-40 and NCEP 100 hPa temperatures, and the anomalies of the lapse-rate tropopause temperature (over 15°S to 15°N) from radiosondes as published by Seidel *et al.* [2001]. Figures A1c–A1g show the temperature difference between monthly mean 100 hPa radiosonde temperatures (as provided by the SPARC data center at <http://www.sparc.sunysb.edu/>) at selected stations minus the corresponding (in pressure/longitude/latitude) monthly mean ERA-40 temperature. The stations shown here were selected because of their generally good data quality (as discussed by Seidel *et al.* [2001]) and their relevance for $[\text{H}_2\text{O}]_e$, which the model calculations used here find to be largely controlled by temperatures over the western Pacific. The data from Ascension were selected to round off global coverage.

[75] The overall comparison in Figure A1b suggests that ERA-40 has a 1–2 K cold bias with respect to the radiosondes during the period 1979–1985. This is seen consistently in Figures A1c–A1g across the individual radiosondes, and consequently it is expected that the Lagrangian cold point shows a similar bias. Figure A1b further indicates that ERA-40 has a smaller cold bias (1 K) during 1986–1988, which is also apparent at Majuro and Kota Kinabula, but not, for example, at Songkhla. The significance of this latter bias for Lagrangian cold point calculations is therefore difficult to assess.

[76] The difference between NCEP and ERA-40 temperature anomalies (Figure A1b) from about 1998 onward reflect the temperature drift in NCEP data in the 1990s relative to ERA-40 (as also seen in Figure A1a). The radiosonde data shown here end in 1997, but the comparison with radiosondes shown by Simmons [2003] shows that ERA-40 remains in very good agreement with radiosondes until 2002.

[77] We further note that the comparison of interannual anomalies of radiosonde tropical mean cold point tropopause temperatures with those of ERA-40 100 hPa temperatures shown by Randel *et al.* [2004, Figure 13] shows warm biases of ERA-40 temperatures with respect to radiosondes of about 0.5 K in 1991 and from 1993 to 1994, which are not obvious in the comparisons shown in Figure A1.

[78] The generally good agreement of ERA-40 temperatures with radiosondes shows that ERA-40 captures the

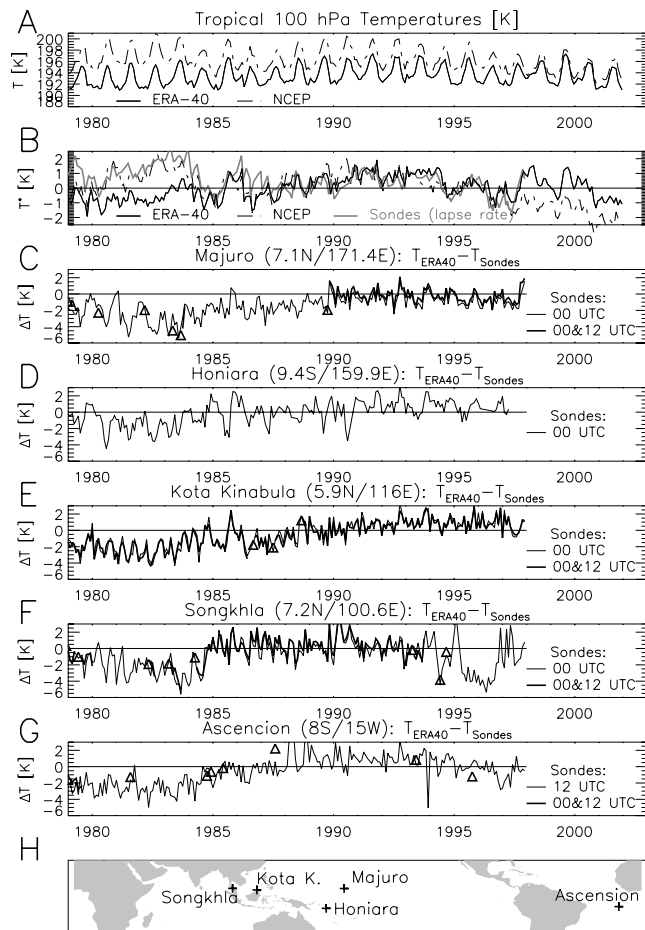


Figure A1. Comparison of monthly mean temperatures at 100 hPa. (a) Tropical mean (10°S to 10°N) temperature from ERA-40 (solid line) and NCEP (dash-dotted line); (b) Deseasonalized temperature anomalies of tropical mean temperature from ERA-40 (black solid line) and NCEP (dash-dotted line), and of tropical lapse rate tropopause temperatures from radiosondes (grey solid line) as published by Seidel *et al.* [2001] (shifted by 0.5 K to match ERA-40 in the 1990s). (c–g) Temperature difference between ERA-40 and observed radiosonde temperatures as published by Seidel *et al.* [2001]; locations are shown in Figure A1h. Thin lines, difference of monthly mean ERA-40 (diurnal mean) temperature minus observation at indicated UTC; solid lines, difference ERA-40 (diurnal mean) temperature minus average of 0000 UTC and 1200 UTC observations. Triangles show values for single months when both 0000 UTC and 1200 UTC data are available.

tropical tropopause temperatures better than the NCEP data, but has apparently a cold bias over the period 1979–1985, and temperatures appear suspect during 1986–1987 and perhaps over some shorter periods in the early 1990s.

[79] **Acknowledgments.** We thank MeteoSwiss for providing ERA-40 data and H. Wernli for the trajectory code LAGRANTO. We thank NASA Langley Research Center (NASA-LaRC) and the NASA Langley Radiation and Aerosols Branch for providing the SAGE II data. We thank M. Baker for helpful comments on an earlier version of this paper, L. Thomason for helpful comments on the SAGE II v6.2 water vapor data, H. Vömel for providing the NOAA water vapor measurements over

Boulder, Colorado, and information about accuracies and measurement technique, and W. J. Read for providing the MLS V7.02 water vapor measurements. S.F. has been supported by NASA grants NNG04GM23G and 6524 Aura/HIRDLS. P.H.H. acknowledges support from the UK Natural Environment Research Council (grant GST/02/2829), the Isaac Newton Trust, and the EU through the SCOUT-03 Integrated Project.

References

- Baldwin, M. P., et al. (2001), The quasi-biennial oscillation, *Rev. Geophys.*, **39**, 179–229.
- Bluth, G. J. S., S. D. Doiron, C. C. Schnetzler, A. J. Krueger, and L. S. Walter (1992), Global tracking of the SO_2 clouds from the June, 1991 Mount Pinatubo eruptions, *Geophys. Res. Lett.*, **19**, 151–154.
- Bonazzola, M., and P. H. Haynes (2004), A trajectory-based study of the tropical tropopause region, *J. Geophys. Res.*, **109**, D20112, doi:10.1029/2003JD004356.
- Danielsen, E. F. (1993), In situ evidence of rapid, vertical, irreversible transport of lower tropospheric air into the lower tropical stratosphere by convective cloud turrets and by larger-scale upwelling in tropical cyclones, *J. Geophys. Res.*, **98**, 8665–8681.
- Dlugokencky, E. J., K. A. Masarie, P. M. Lang, and P. P. Tans (1998), Continuing decline in the growth rate of the atmospheric methane burden, *Nature*, **393**, 447–450.
- Dvortsov, V. L., and S. Solomon (2001), Response of the stratospheric temperatures and ozone to past and future increases in stratospheric humidity, *J. Geophys. Res.*, **106**, 7505–7514.
- Etheridge, D. M., G. I. Pearman, and P. J. Fraser (1992), Changes in tropospheric methane between 1841 and 1978 from a high accumulation-rate Antarctic ice core, *Tellus, Ser. B*, **44**, 282–292.
- Evans, S. J., R. Toumi, J. E. Harries, M. P. Chipperfield, and J. M. Russell III (1998), Trends in stratospheric humidity and the sensitivity of ozone to these trends, *J. Geophys. Res.*, **103**, 8715–8725.
- Forster, P. M. de F., and K. Shine (2002), Assessing the climate impact of trends in stratospheric water vapour, *Geophys. Res. Lett.*, **29**(6), 1086, doi:10.1029/2001GL013909.
- Fueglistaler, S., H. Wernli, and T. Peter (2004), Tropical troposphere-to-stratosphere transport inferred from trajectory calculations, *J. Geophys. Res.*, **109**, D03108, doi:10.1029/2003JD004069.
- Fueglistaler, S., M. Bonazzola, P. H. Haynes, and T. Peter (2005), Stratospheric water vapor predicted from the Lagrangian temperature history of air entering the stratosphere in the tropics, *J. Geophys. Res.*, **110**, D08107, doi:10.1029/2004JD005516.
- Geller, M., X. Zhou, and M. Zhang (2002), Simulations of the interannual variability of stratospheric water vapour, *J. Atmos. Sci.*, **59**, 1076–1085.
- Gettelman, A., W. J. Randel, S. Massie, F. Wu, W. G. Read, and J. M. Russell III (2001), El Niño as a natural experiment for studying the tropical tropopause region, *J. Clim.*, **14**, 3375–3391.
- Giorgetta, M. A., and L. Bengtsson (1999), Potential role of the quasi-biennial oscillation in the stratosphere-troposphere exchange as found in water vapor in general circulation model experiments, *J. Geophys. Res.*, **104**, 6003–6019.
- Hatsushika, H., and K. Yamazaki (2003), Stratospheric drain over Indonesia and dehydration within the tropical tropopause layer diagnosed by air parcel trajectories, *J. Geophys. Res.*, **108**(D19), 4610, doi:10.1029/2002JD002986.
- Held, I. M., and B. J. Soden (2000), Water vapor feedback and global warming, *Annu. Rev. Energy Environ.*, **25**, 441–475.
- Holton, J. R. (1990), On the global exchange of mass between the stratosphere and troposphere, *J. Atmos. Sci.*, **47**, 392–395.
- Holton, J. R., and A. Gettelman (2001), Horizontal transport and the dehydration of the stratosphere, *Geophys. Res. Lett.*, **28**, 2799–2802.
- Holton, J. R., P. H. Haynes, M. E. McIntyre, A. R. Douglass, R. B. Rood, and L. Pfister (1995), Stratosphere-troposphere exchange, *Rev. Geophys.*, **33**, 403–440.
- Kalnay, E., et al. (1996), The NCEP/NCAR 40-year reanalysis project, *Bull. Am. Meteorol. Soc.*, **77**, 437–471.
- Kinnersley, J. S., and S. Pawson (1996), The descent rates of the shear zones of the equatorial QBO, *J. Atmos. Sci.*, **53**, 1937–1949.
- Kinnison, D. E., K. E. Grant, P. S. Connell, D. A. Rotman, and D. J. Wuebbles (1994), The chemical and radiative effects of the Mount Pinatubo eruption, *J. Geophys. Res.*, **99**, 25,705–25,731.
- Kley, D., J. M. Russell III, and C. Phillips (Eds.) (2000), SPARC assessment of upper tropospheric and stratospheric water vapour, *WCRP 113, WMO/TD 1043, SPARC Rep. 2*, World Meteorol. Organ., Geneva.
- Lanzante, J. R., S. A. Klein, and D. J. Seidel (2003), Temporal homogenization of monthly radiosonde temperature data. Part II: Trends, sensitivities, and MSU comparison, *J. Clim.*, **16**, 241–262.
- Le Texier, H., S. Solomon, and R. R. Garcia (1988), The role of molecular hydrogen and methane oxidation in the water vapor budget of the stratosphere, *Q. J. R. Meteorol. Soc.*, **114**, 281–295.

- Michelsen, H. A., R. W. Irion, G. L. Manney, G. C. Toon, and M. R. Gunson (2000), Features and trends in Atmospheric Trace Molecule Spectroscopy (ATMOS) version 3 stratospheric water vapor and methane measurements, *J. Geophys. Res.*, *105*, 22,713–22,724.
- Newell, R. E., and S. Gould-Stewart (1981), A stratospheric fountain?, *J. Atmos. Sci.*, *38*, 2789–2796.
- Notholt, J., et al. (2005), Influence of tropospheric SO₂ emissions on particle formation and the stratospheric humidity, *Geophys. Res. Lett.*, *32*, L07810, doi:10.1029/2004GL022159.
- Oltmans, S. J., H. Vömel, D. J. Hofmann, K. H. Rosenlof, and D. Kley (2000), The increase in stratospheric water vapor from balloonborne, frost-point hygrometer measurements at Washington, D. C., and Boulder, Colorado, *Geophys. Res. Lett.*, *27*, 3453–3456.
- Randel, W. J., F. Wu, J. M. Russell III, A. Roche, and J. W. Waters (1998), Seasonal cycles and QBO variations in stratospheric CH₄ and H₂O observed in UARS HALOE data, *J. Atmos. Sci.*, *55*, 163–185.
- Randel, W. J., F. Wu, R. Swinbank, J. Nash, and A. O'Neill (1999), Global QBO circulation derived from UKMO stratospheric analyses, *J. Atmos. Sci.*, *56*, 457–474.
- Randel, W. J., F. Wu, S. J. Oltmans, K. Rosenlof, and G. E. Nedoluha (2004), Interannual variability of stratospheric water vapor and correlations with tropical tropopause temperatures, *J. Atmos. Sci.*, *61*, 2133–2148.
- Read, W. G., D. L. Wu, J. W. Waters, and H. C. Pumphrey (2004), A new 147–56 hPa water vapor product from the UARS Microwave Limb Sounder, *J. Geophys. Res.*, *109*, D06111, doi:10.1029/2003JD004366.
- Rosenlof, K. H. (2002), Transport changes inferred from HALOE water and methane measurements, *J. Meteorol. Soc. Jpn.*, *80*(4B), 831–848.
- Rosenlof, K. H., et al. (2001), Stratospheric water vapor increases over the past half-century, *Geophys. Res. Lett.*, *28*, 1195–1198.
- Russell, J. M., III, A. F. Tuck, L. L. Gordley, J. H. Park, S. R. Drayson, J. E. Harries, R. J. Cicerone, and P. J. Crutzen (1993), The Halogen Occultation Experiment, *J. Geophys. Res.*, *98*, 10,777–10,797.
- Scaife, A. A., N. Butchard, D. R. Jackson, and R. Swinbank (2003), Can changes in ENSO activity help to explain increasing stratospheric water vapor?, *Geophys. Res. Lett.*, *30*(17), 1880, doi:10.1029/2003GL017591.
- Seidel, D. J., R. J. Ross, J. K. Andell, and G. C. Reid (2001), Climatological characteristics of the tropical tropopause as revealed by radiosondes, *J. Geophys. Res.*, *106*, 7857–7878.
- Sherwood, S. C. (2002), A microphysical connection among biomass burning, cumulus clouds, and stratospheric moisture, *Science*, *295*, 1272–1275.
- Sherwood, S. C., and A. E. Dessler (2000), On the control of stratospheric humidity, *Geophys. Res. Lett.*, *27*, 2513–2516.
- Simmons, A. J. (2003), Representation of the stratosphere in ECMWF operations and ERA-40, paper presented at ECMWF/SPARC Workshop on Modelling and Assimilation for the Stratosphere and Tropopause, Eur. Cent. for Medium-Range Weather Forecasts, Reading, UK, 23–26 June.
- Simmons, A. J., and J. K. Gibson (2000), The ERA-40 Project plan, *ERA-40 Proj. Rep. Ser. 1*, 63 pp., Eur. Cent. for Medium-Range Weather Forecasts, Reading, UK.
- Thomason, L. W., S. P. Burton, N. Iyer, J. M. Zawodny, and J. Anderson (2004), A revised water vapor product for the Stratospheric Aerosol and Gas Experiment (SAGE) II version 6.2 data set, *J. Geophys. Res.*, *109*, D06312, doi:10.1029/2003JD004465.
- Waugh, D. W., and T. M. Hall (2002), Age of stratospheric air: Theory, observations, and models, *Rev. Geophys.*, *40*(4), 1010, doi:10.1029/2000RG000101.
- Zhou, X., M. A. Geller, and M. Zhang (2001), Cooling trend of the tropical cold point tropopause temperatures and its implications, *J. Geophys. Res.*, *106*, 1511–1522.
- Zöger, M., A. Engel, D. S. McKenna, C. Schiller, U. Schmidt, and T. Woyke (1999), Balloon-borne in situ measurements of stratospheric H₂O, CH₄ and H₂ at midlatitudes, *J. Geophys. Res.*, *104*, 1817–1825.

S. Fueglistaler, Department of Atmospheric Sciences, University of Washington, Box 351640, Seattle, 98195-1640, USA. (stefan@atmos.washington.edu)

P. H. Haynes, Department of Applied Mathematics and Theoretical Physics, Centre for Mathematical Sciences, University of Cambridge, Wilberforce Road, Cambridge CB3 0WA, UK.